General description of fission observables: The GEF code

Karl-Heinz Schmidt[1,⋆], *Beatriz* Jurado[1,⋆⋆], and *Christelle* Schmitt[2,⋆⋆⋆]

[1] *CENBG, CNRS/IN2 P3, Chemin du Solarium B.P. 120, F-33175 Gradignan, France*
[2] *GANIL, Bd. Henri Becquerel, B.P. 55027, F-14076 Caen Cedex 05, France*

Abstract. The GEF model code is described. It has been developed during the last years with the aim to cover practically all fission quantities of a large number of fissioning systems over a wide range of excitation energy with a semi-empirical description without the need for further adjustment to experimental data of specific systems. The basic theoretical ideas and the method of the parameter determination are explained, a short overview on selected results is given, and the application for evaluation and validation of nuclear data is demonstrated with a few examples.

1 Introduction

This contribution is dedicated to the presentation of a general description of fission observables (the GEF model code) and its application in the domain of nuclear data. The model is characterized by a number of theoretical ideas and hypotheses that form a firm frame, linking practically all fission quantities of all fissioning systems among each other. These links include not only the different fission quantities of one fissioning system, but also their variation with the mass, nuclear charge, excitation energy, and angular momentum of the fissioning system. This theoretical frame allows to trace back the values of practically all fission quantities of hundreds of fissioning systems over the large energy range from spontaneous fission up to excitation energies of 100 MeV to a consistent description with only about 100 parameters. These parameters have physical meaning, like energies, temperatures and oscillator frequencies. The values of these parameters have been determined by adjustment to the large body of relevant empirical data.

The GEF model combines to some extent the good reproduction of experimental data obtained by purely empirical models (e.g. ref. [1]) with the predictive power of stochastic models (based on the numerical solution of the Langevin equations or the random-walk approach) (e.g. ref. [2, 3]), or fully microscopic self-consistent models (e.g. ref. [4]). Of course, the GEF model misses the microscopic basis, but, due to its theoretical frame with adjusted parameter values, it allows a generalization of the empirical information in an extended region not too far from well investigated systems. This is comparable to the liquid-drop model, which is still the basis for the most accurate atomic-mass values provided by the macroscopic-microscopic approach [5]. Additional assets of the GEF model are the consistent description of nearly all fission quantities with their correlations, while the empirical systematics only provide separate descriptions of the different observables, and the stochastic and the self-consistent models are presently restricted to a rather small number of about 4 or 5 degrees of freedom that can explicitly be treated.

The present article focuses on the dependences of the different fission quantities and the method of parameter determination in order to understand the ability of the GEF model to provide reliable predictions for fissioning nuclei for which no experimental data exist. Moreover, the ability to establish covariances and its suitability for validation and evaluation are illustrated. A comprehensive documentation of the GEF model code can be found elsewhere [6].

⋆ e-mail: schmidt-erzhausen@t-online.de
⋆⋆ e-mail: jurado@cenbg.in2p3.fr
⋆⋆⋆ e-mail: schmitt@ganil.fr

2 Theoretical ideas and hypotheses

In this section, some of the main theoretical ideas and hypotheses of the GEF model are listed.

2.1 Fission barriers

Fission barriers are calculated by use of the topographic theorem [7] as the sum of the macroscopic barrier and the additional binding energy by the empirical ground-state shell correction. This approach avoids the uncertainties of the theoretical shell-correction energies and allows to discriminate between different macroscopic models [8].

2.2 Fission channels

The fission channels are related to the statistical population of quantum oscillators in the mass-asymmetry degree of freedom that form the fission valleys. The quantum oscillator of each channel is characterized by three parameters (position, depth, and curvature) that are traced back

to the macroscopic potential (symmetric fission channel SL) and to shells in the proton and neutron subsystems of both fragments (fission channels S1 and S2), which are assumed to be effective already little beyond the outer saddle [9]. These shells are assumed to be the same for all fissioning systems. It is the superposition of different shells and the interaction with the macroscopic potential that create the mass distributions which differ for different systems [10]. These shells also determine the shapes (mainly the quadrupole deformation) of the nascent fragments at scission. According to Strutinsky-type calculations, the fragment shapes are found to be a linearly increasing function of the number of protons, respectively neutrons, in regions between closed spherical shells [11]. Also the charge-polarization (deviation of the N/Z degree of freedom at scission - mean value and fluctuations - from the 'UCD' value of the fissioning nucleus) is treated by the corresponding quantum oscillator [12].

2.3 Energy sorting

By the influence of pairing correlations, the nuclear temperature below the critical pairing energy is assumed to be constant [13]. Therefore, the di-nuclear system between saddle and scission consists of two coupled microscopic thermostates [14]. This leads to a sorting process of the available intrinsic energy and of unpaired nucleons before scission [15–17].

3 Method of parameter determination

In this section, the main aspects of the parameter determination are described. They illustrate the far-reaching influence of a specific model parameter on different observables in nearly all fissioning systems. The parameters were determined by minimizing the deviations of the model from measured fission-fragment A distributions, independent yields, isomeric ratios, total kinetic energies (TKEs), and the multiplicities of prompt and delayed neutrons, and the dependencies between these quantities. We restrict ourselves in the following to the properties of the three most intense fission channels. More details and the specific numerical values of the parameters are found in ref. [6].

3.1 Location of fission channels

According to Strutinsky-type calculations [11], the asymmetric fission channel S1 is caused by the spherical shell closures in $Z = 50$ and $N = 82$, and the S2 channel, which has the largest yield in the actinides, is related to a shell near $N = 88$ at large deformation ($\beta \approx 0.5$). Therefore, one expects that the S1 fission channel is located near $A = 132$, while the S2 channel appears close to $N = 88$. A detailed analysis of available A and Z distributions, however, revealed that the S1 and the S2 channels appear close to $Z = 52$ and $Z = 55$, respectively, and that A and N vary accordingly with the size of the fissioning system, see figure 1. This unexpected result is taken as an empirical information without a deeper understanding at this time.

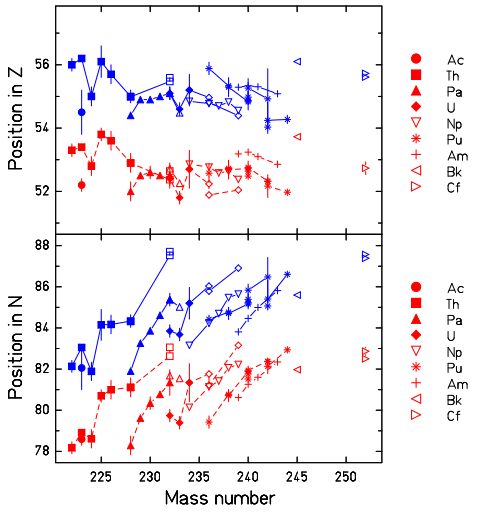

Figure 1. Mean positions of the standard S1 and S2 fission channels in atomic number (upper part) and neutron number (lower part) deduced from measured fission-fragment A and Z distributions. The shape of the symbol denotes the element as given in the legend of the figure. Data from ref. [18] are marked by solid symbols. The values of S1 (S2) for the isotopes of a given element are connected by dashed (full) lines and marked by red (blue) symbols. The figure is taken from ref. [18].

3.2 Yields and shapes of fission channels

The yield of a specific fission channel is expected to be proportional to the exponential of the binding energy at the bottom of the respective fission channel. Indeed, a good description of the relative yields of the fission channels is obtained, when the depth of the S1 fission valley decreases approximately as a linear function with increasing distance of the N/Z of the fissioning system from the N/Z value of ^{132}Sn, while the depth of the S2 fission valley with respect to the macroscopic potential is the same for all systems.

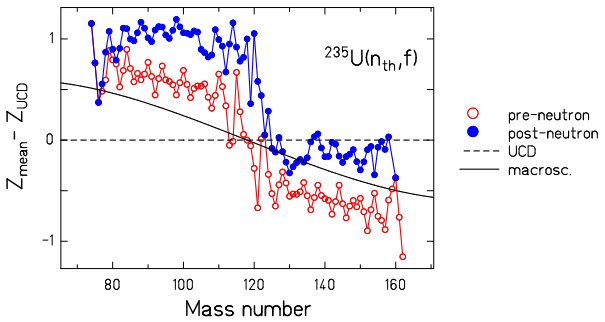

Figure 2. Deviation of the mean nuclear charge of isobaric chains from the UCD value for different cases for the system ^{235}U(n$_{th}$,f). Dashed line: UCD value. Full line: Macroscopic value at scission. Open symbols: Values from GEF before prompt-neutron emission as a function of pre-neutron mass. Full symbols: Values from GEF after prompt-neutron emission as a function of post-neutron mass. The figure is taken from ref. [6].

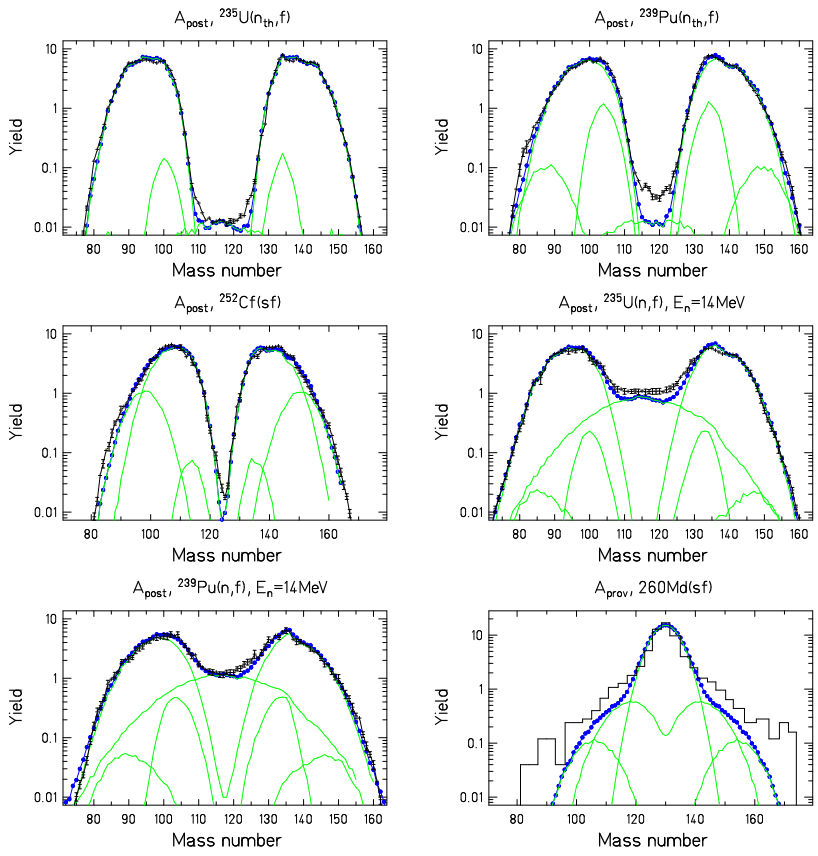

Figure 3. Evaluated [19] and measured [20] mass distributions (black symbols) of fission fragments in comparison with the result of the GEF model (blue symbols). The green lines show the calculated contributions from the different fission channels (SL, S1, S2, and the super-asymmetric fission channel SA). The figure is taken from ref. [21] with kind permission of The European Physical Journal (EPJ). For details see ref. [21].

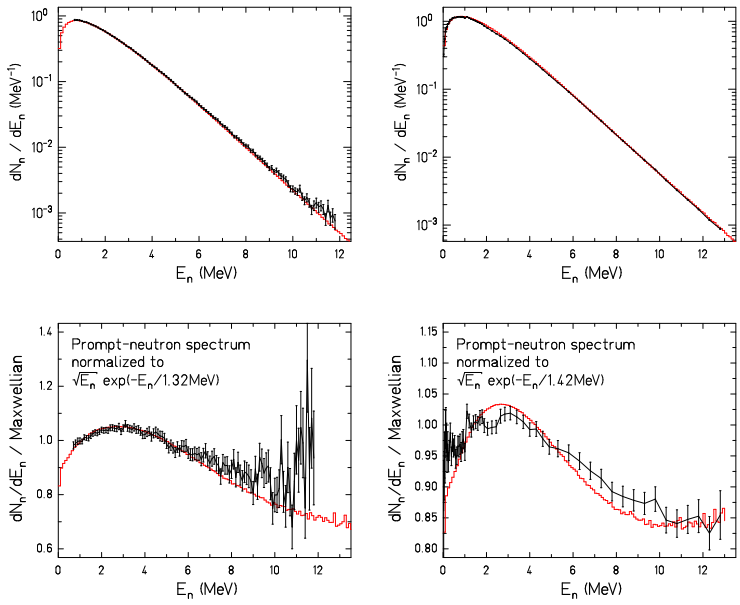

Figure 4. Upper panels: Experimental prompt-fission-neutron energy spectra (black lines and error bars) for ^{235}U(n$_{th}$,f) [22] (left part) and ^{252}Cf(sf) [23] (right part) in comparison with the result of the GEF model (red histograms) in logarithmic scale. In the lower panels, the spectra have been normalized to a Maxwellian with T = 1.32 MeV and T = 1.42 MeV, respectively. The figure is modifed from ref. [6].

The shapes of the mass distributions are well described by assuming a Gaussian for the S1 channel and a rectangle convoluted with a Gaussian for the S2 channel. This implies that the width of the rectangle appears as an additional parameter.

3.3 Shapes of the nascent fragments

The fragment-mass dependence of the prompt-neutron multiplicities is well described by assuming the same linear dependence of the quadrupole deformation with the number of protons in the nascent fragments for all fissioning systems. This is consistent with the constant position of the fission channels in Z, as mentioned above. It explains also the major part of the increasing prompt-neutron multiplicity, for example from ^{235}U(n$_{th}$,f) to ^{252}Cf(sf), due to the enhanced production of fragments on the right wing of the light fragment component.

3.4 Charge polarization

There is no direct experimental information available on the charge polarization at scission, but it can be determined indirectly. Figure 2 demonstrates, how the experimentally accessible $Z_{mean} - Z_{UCD}$ values as a function of post-neutron mass are linked by the mass-dependent prompt-neutron multiplicity to the $Z_{mean} - Z_{UCD}$ values (the charge polarization at scission) as a function of pre-neutron mass. The trend of the latter quantity follows the macroscopic values in the light and the heavy fragment group, but an additional roughly constant polarization that shifts the light fragments to more neutron-deficient and the heavy fragments to more neutron-rich isotopes is necessary to reproduce the experimental post-neutron values.

4 Selected results

In this section, some typical results of the GEF code are presented and, if available, compared with measured or evaluated data.

4.1 Fission-fragment yields

In figure 3, calculated mass distributions are compared with empirical data for a few selected systems. The Chi-squared deviations between GEF results and the evaluation of ref. [19] for all mass distributions are shown in figure 5. The majority of the Chi-squared values are close to unity, demonstrating the good reproduction of the data by the GEF model. Most of the large Chi-squared values are caused by issues in the evaluation (see ref. [6]). Some of those will be considered more closely in section 5.

4.2 Prompt-neutron emission

The energy spectra of the prompt neutrons are well reproduced by the GEF model without further adjustments. Figure 4 shows a comparison for the two systems with the best experimental information. Critical ingredients like level densities and transmission coefficients are directly taken from literature (see ref. [6]). Also the gamma competition, which has an additional influence on the shape of the prompt-neutron spectrum, is treated without specific adjustments [6].

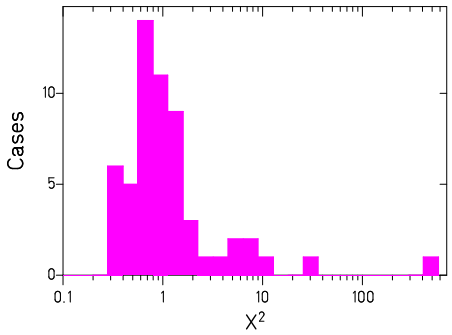

Figure 5. Chi-squared deviations of 57 mass distributions calculated with GEF from evaluated data [19] in a logarithmic binning. The height of the histogram represents the number of cases per bin. The figure is taken from ref. [6].

Table 1. Mean properties of prompt and delayed neutrons. (E_n is the incoming-neutron energy. Mean energy E_{prompt} and multiplicity ν_{prompt} refer to prompt neutrons emitted from the fragments. The decay data from JEFF 3.1.1 were used to calculate $\nu_{delayed}$.)

System	E_n [MeV]	E_{prompt} [MeV]	ν_{prompt}	$\nu_{delayed}$
^{233}U(n,f)	thermal	2.02(1)	2.36(1)	0.77(9)
^{233}U(n,f)	5	2.06(1)	3.10(2)	0.79(16)
^{235}U(n,f)	thermal	2.00(1)	2.42(2)	1.60(10)
^{235}U(n,f)	5	2.06(1)	3.18(2)	1.48(12)
^{238}U(n,f)	5	2.01(1)	3.05(2)	3.51(14)
^{237}Np(n,f)	thermal	2.02(1)	2.38(6)	1.47(7)
^{237}Np(n,f)	5	2.08(1)	3.12(2)	1.05(5)
^{238}Np(n,f)	thermal	2.02(1)	2.57(6)	1.82(15)
^{238}Np(n,f)	5	2.09(1)	3.36(3)	1.40(7)
^{239}Pu(n,f)	thermal	2.08(1)	2.80(4)	0.68(4)
^{239}Pu(n,f)	5	2.13(1)	3.57(5)	0.61(3)
^{241}Pu(n,f)	thermal	2.06(1)	2.88(5)	1.42(5)
^{241}Pu(n,f)	5	2.12(2)	3.70(4)	1.16(5)
^{252}Cf(s,f)	——	2.16(2)	3.76(2)	0.76(12)

Table 1 lists calculated average quantities of the prompt and the delayed neutrons for a few selected systems. The uncertainties refer only to the uncertainties of the parameters of the GEF model, which are specific to the fission process. Additional uncertainties, for example by the nuclear level density or the decay data, are not included.

As expected from the good reproduction of the prompt-neutron energy spectra in figure 4, the mean prompt-neutron energies for ^{233,235}U(n$_{th}$,f) and ^{239}Pu(n$_{th}$,f) agree with the recent evaluation of ref. [24] within the estimated error bars.

The prompt-neutron multiplicities for ^{235}U(n$_{th}$,f), ^{239,241}Pu(n$_{th}$,f), ^{252}Cf(sf), ^{238}U(n,f) and ^{239}Pu(n,f) with

Table 2. Mean properties of prompt gamma emission. (E_n is the incoming-neutron energy, E_γ and N_γ are the average gamma energy and multiplicity, and E_{tot} is the total gamma energy in one fission event.)

System	E_n [MeV]	E_γ [MeV]	N_γ	E_{tot}
^{233}U(n,f)	thermal	1.00(2)	6.8(5)	6.75(40)
^{233}U(n,f)	5	1.00(1)	7.4(4)	7.38(33)
^{235}U(n,f)	thermal	0.94(1)	6.9(3)	6.44(20)
^{235}U(n,f)	5	0.94(1)	7.5(4)	7.03(27)
^{238}U(n,f)	5	0.87(2)	7.1(4)	6.21(27)
^{237}Np(n,f)	thermal	0.94(2)	6.8(5)	6.42(33)
^{237}Np(n,f)	5	0.94(2)	7.3(6)	6.89(38)
^{238}Np(n,f)	thermal	0.92(3)	6.8(6)	6.27(35)
^{238}Np(n,f)	5	0.92(2)	7.4(5)	6.78(31)
^{239}Pu(n,f)	thermal	0.94(1)	6.9(3)	6.54(18)
^{239}Pu(n,f)	5	0.94(1)	7.5(4)	7.09(26)
^{241}Pu(n,f)	thermal	0.90(2)	7.0(4)	6.23(27)
^{241}Pu(n,f)	5	0.90(2)	7.6(6)	6.81(38)
^{252}Cf(s,f)	——	0.85(2)	7.2(3)	6.14(14)

E_n=5 MeV agree with the evaluated data (ENDF/B-VII.1, [25, 26]) within the estimated error bars or slightly beyond. The values for ^{233}U(n_{th},f) and ^{237,238}Np(n_{th},f) deviate by up to 0.2 units. These discrepancies should be considered in a more comprehensive analysis, may be including a re-examination of the data underlying the evaluations.

4.3 Prompt-gamma emission

The most important quantity related to prompt-gamma emission in nuclear-reactor technology is the total gamma energy per fission event. Table 2 lists this quantity together with the mean gamma energy and the gamma multiplicity per fission as calculated with the GEF code. The uncertainties of the multiplicities and total energies are mostly caused by an assumed uncertainty of 10 % (standard deviation) in the fragment angular momenta. The values that can be compared with experimental data agree within the given uncertainties and the scattering of the experimental values (see e.g. tables XIV, XV and XVI of ref. [6])[1]. Only the gamma multiplicity (and in consequence the total gamma energy) for ^{252}Cf(sf) is systematically too low by about 10 %. This problem that is probably caused by underestimated fragment angular momenta for this system requires further investigation.

4.4 Isomeric ratios

Many isomers exist among the fission products and play an important role for the calculation of the decay heat after reactor shutdown. Furthermore, the beta-delayed neutron-emission probability from the isomeric state can be an order of magnitude different from that of the ground state. Thus, proper simulation of the effect of delayed neutrons in reactors requires accurate knowledge of the population of isomeric states in fission. Measurements of isomeric yield ratios are also important for simulations of the astrophysical r-process. The isomeric ratio (IR) predicted by the GEF model depends on the properties of the fissioning nucleus, namely its excitation energy and spin, as well as on the properties of the fission fragment, that are its mass, Z, deformation, and difference between its isomeric-state and ground-state spins and binding energies. In the GEF code, it is essentially assumed that the angular momentum of the fragments is created by the statistical population of single-particle and collective states according to the fragment temperature at scission. The energies and spins of the isomeric states as possibly populated in the calculations are taken from empirical data.

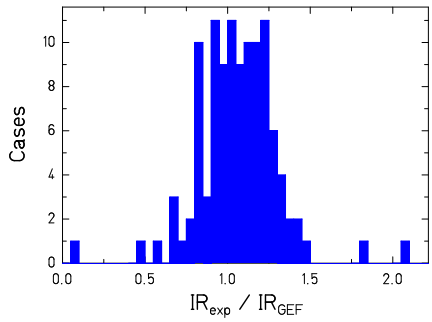

Figure 6. Distribution of the ratio between the experimental and calculated IR for several tens of fragment isomers and fissioning nuclei.

The achievement of GEF for IRs is summarized in figure 6, where the distribution of the ratio between the experimental and calculated IR is shown, including a large sample of representative fragment isomeric states and fissioning systems. It demonstrates the good description of this observable by the code. A further critical discussion can be found in [6].

5 Application for validation and evaluation

In this section, the use of GEF for validation and evaluation of fission data is demonstrated with a few examples. More examples can be found in ref. [6].

Figure 7 shows a comparison of the fission-fragment mass distribution of ^{237}Np(n_{th},f) from ENDF/B-VII in comparison with the GEF result. The discrepancies in the light-fragment group can be explained by a contamination of the ^{237}Np target with a contribution of 15 ppm of ^{239}Pu, as demonstrated in the lower part.

Another indication for an erroneous evaluation result, probably due to scarce data, is shown in figure 8. There is an appreciable shift in the position of the light fragment peak, and the mean value of the mass spectrum of 126.5 lets only room for the emission of 2 prompt neutrons, while a value of 4.91 is expected from GEF.

[1] The values of the total gamma energy given in ref. [6] are not correct and should be replaced by the values given in table 2.

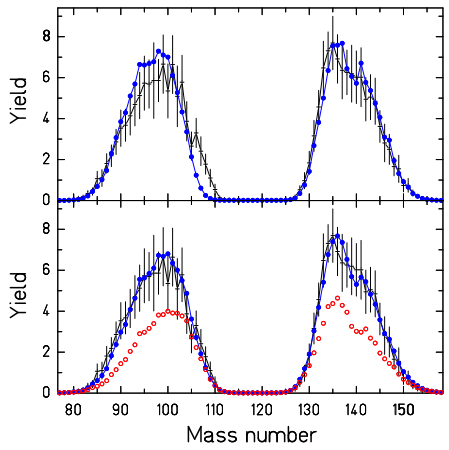

Figure 7. Evidence for a Pu contaminant in a ^{237}Np target. The fission-fragment mass distribution of the system ^{237}Np(n$_{th}$,f) from ref. [19] and ENDF/B-VII (black crosses with error bars) in comparison with the result of the GEF code for a pure ^{237}Np target (upper figure, blue full points) and for a composite target (40 % fission from ^{237}Np and 60 % fission from ^{239}Pu) (lower figure, blue full points). In addition, the contribution from the assumed ^{239}Pu contaminant is shown separately in the lower figure (open red symbols). The figure is taken from ref. [6].

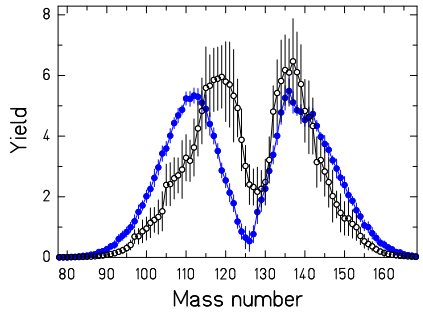

Figure 8. Fission-fragment mass distribution of ^{255}Fm(n$_{th}$,f) from ref. [19] and ENDF/B-VII (black open symbols) compared with the GEF result (full blue symbols)

6 Conclusion

The GEF code reproduces a large variety of fission observables with a good precision in a consistent way without further adjustment to specific fissioning systems. With this global approach, the model is able to predict essentially all the observables associated to the fission process. In contrast to most existing models, GEF is able to provide accurate predictions for fissioning nuclei for which no experimental data are available. The consistent description of all fission quantities permits establishing correlations between all of them and makes the model a valuable tool for application in validation and evaluation of nuclear data.

Acknowledgement

The development of the GEF model code has been supported by the Nuclear-Energy Agency of the OECD as well as by the European Commission within the Sixth Framework Programme through EFNUDAT (project no. 036434), within the Seventh Framework Programme through Fission-2010- ERINDA (project no. 269499), and CHANDA (project no. 605203), and by the GSI/IN2P3-CNRS collaboration agreement 04-48.

References

[1] A. C. Wahl, Report LA-13928 (Los Alamos National Laboratory, 2002)
[2] M. D. Usang et al., Phys. Rev. C **94**, 044602 (2016)
[3] J. Randrup and P. Möller, Phys. Rev. C **88**, 064606 (2013)
[4] D. Regnier, N. Dubray, N. Schunck, and M. Verriere, Phys. Rev. C **93**, 054611 (2016)
[5] A. Sobiczewski, Y. A. Litvinov, Phys. Rev. C **89**, 024311 (2014)
[6] K.-H. Schmidt, B. Jurado, Ch. Amouroux, and Ch. Schmitt, Nucl. Data Sheets **131**, 107 (2016)
[7] W. D. Myers and W. J. Swiatecki, Nucl. Phys. A **601**, 14 (1996)
[8] A. Kelić and K.-H. Schmidt, Phys. Lett. B **634** (2006) 362
[9] U. Mosel and H. W. Schmitt, Nucl. Phys. A **165**, 73 (1971)
[10] K.-H. Schmidt, A. Kelić, and M. V. Ricciardi, Europh. Lett. **83**, 32001 (2008)
[11] B. D. Wilkins, E. P. Steinberg, and R. R. Chasman, Phys. Rev. C **14**, 1832 (1976)
[12] H. Nifenecker, J. Physique Lett. **41**, 47 (1980)
[13] K.-H. Schmidt and B. Jurado, Phys. Rev. C **86**, 044322 (2012)
[14] K.-H. Schmidt and B. Jurado, Phys. Rev. Lett. **104**, 212501 (2010)
[15] K.-H. Schmidt and B. Jurado, Phys. Rev. C **83**, 014607 (2011)
[16] K.-H. Schmidt and B. Jurado, Phys. Rev. C **83**, 061601 (2011)
[17] B. Jurado and K.-H. Schmidt, J. Phys. G: Nucl. Part. Phys. **42**, 055101 (2015)
[18] C. Böckstiegel et al., Nucl. Phys. A **802**, 12 (2008)
[19] T. R. England and B. F. Rider, Report ENDF-349, LA-UR-94-3106 (Los Alamos National Laboratory, 1994)
[20] E. K. Hulet et al., Phys. Rev. C **40**, 770 (1989)
[21] K.-H. Schmidt and B. Jurado, Eur. Phys. J. A **51**, 176 (2015)
[22] N. V. Kornilov et al., Nucl. Sci. Eng. **165**, 117 (2010)
[23] W. Mannhart, INDC(NDS)-220 (1989) 305, IAEA, Vienna
[24] R. Capote et al., Nucl. Data Sheets **131**, 1 (2016)
[25] R. W. Mills, “Fission product yield evaluation", PhD thesis, University of Birmingham, 1995
[26] V. V. Malinovskij, V. G. Vorob’eva, and B. D. Kuz’minov, Report INDC(CCP)-**239**, IAEA, Vienna, Austria, 1985